Published in final edited form as:

Nat Chem Biol. 2018 March ; 14(3): 291–298. doi:10.1038/nchembio.2556.

A Whole Animal Platform to Advance A Clinical Kinase Inhibitor Into New Disease Space

Masahiro Sonoshita[1,5,*], **Alex P. Scopton**[2,*], **Peter M-U. Ung**[3], **Matthew A. Murray**[1,4], **Lisa Silber**[2], **Andres Y. Maldonado**[2], **Alexander Real**[2], **Avner Schlessinger**[3], **Ross L. Cagan**[1,†], and **Arvin C. Dar**[2,†]

[1]Department of Cell, Developmental and Regenerative Biology, Icahn School of Medicine at Mount Sinai, New York, NY 10029

[2]Department of Oncological Sciences, Icahn School of Medicine at Mount Sinai, New York, NY 10029

[3]Department of Pharmacological Sciences, Icahn School of Medicine at Mount Sinai, New York, NY 10029

[4]Department of Biomedical Sciences, Florida State University, Tallahassee, FL 32304

[5]Department of Systems Neuropharmacology, Kyoto University Graduate School of Medicine, Kyoto 606-8501, Japan

Abstract

Synthetic tailoring of approved drugs for new indications is often difficult, as the most appropriate targets may not be readily apparent and therefore few roadmaps exist to guide chemistry. Here, we report a multidisciplinary approach for accessing novel target and chemical space starting from an FDA-approved kinase inhibitor. Combining chemical and genetic modifier screening with computational modeling, we identify distinct kinases that strongly enhance ('pro-targets') or limit ('anti-targets') whole animal activity of the clinical kinase inhibitor sorafenib in a *Drosophila* medullary thyroid carcinoma (MTC) model. We demonstrate that RAF—the original intended sorafenib target—and MKNK kinases function as pharmacological liabilities due to inhibitor-induced transactivation and negative feedback, respectively. Through progressive synthetic refinement, we report a novel class of '*Tumor Calibrated Inhibitor*s' with unique polypharmacology and strongly improved therapeutic index in fly and human MTC xenograft models. This platform provides a rational approach for creating new high efficacy/low toxicity drugs.

†Corresponding authors. arvin.dar@mssm.edu; ross.cagan@mssm.edu.
*These authors contributed equally to this work.

Author Contributions: M.S., A.P.S., R.L.C., and A.C.D. designed research; P.M.U.U. and A.S. designed computational analysis. M.S. designed and conducted functional studies. A.P.S. designed and conducted chemical syntheses. L.S. assisted with chemical synthesis. M.A.M. assisted with *Lk6* genetic analysis. A.Y.M. and A.R. assisted with RAF anti-target analysis in cell lines. All authors analyzed data and M.S., A.P.S., P.M.U.U., A.S., R.L.C., and A.C.D wrote the manuscript.

Competing Financial Interests Statement: M.S., A.P.S., R.L.C., and A.C.D. are inventors on a patent application submitted by the Icahn School of Medicine at Mount Sinai.

Keywords

Drosophila; sorafenib; cancer; polypharmacology

Introduction

Currently, 37 kinase inhibitors (KIs) are FDA-approved for patient use, with these drugs primarily targeting oncogenic kinases. Examples include gleevec for BCR-ABL-mutant leukemia[1] and vemurafenib for BRAF(V600E/K)-mutant melanoma[2]. Advances in sequencing technologies offer the promise that the paradigm of selective inhibitors for mutant kinases would be successfully expanded to wider groups of cancer patients[3]. However, despite extensive efforts, the number of newly identified and actionable kinase mutants has remained relatively small, hindered by the challenges of converting genomic data into therapies[4,5].Overall, success rates of clinical trials for anti-cancer drugs have remained among the lowest for major diseases, with most failures due to limited therapeutic index[6,7]. Additional liabilities can include emergent resistance caused by, for example, mutations within a critical target or feedback responses that alter kinase signaling networks and thereby limit drug efficacy[8].

At the moment, only ~20 out of the more than 500 human kinases are identified as the primary target of a clinical KI[9]. Further, inhibition of a single primary kinase target is often necessary but not sufficient to elicit a therapeutic response[8]. Certainly *in vitro* profiling of KIs suggests secondary 'off-targets' can strongly contribute to biological efficacy[10,11]. Developing complex KI profiles that have emerged as optimal for therapeutics has historically relied on serendipity, whereas physicochemical properties of these compounds are optimized based on well-established parameters[7]. Indeed, the FDA approved set of KIs are highly enriched for 'privileged' chemical structures that provide acceptable bioavailability, distribution, metabolism, and toxicity.

Recognizing a need for biologically optimized KIs that possess novel target profiles and high selectivity for tumors, we previously established a *Drosophila* model of oncogenic RET (*RE*arranged during *T*ransfection) driven MTC to identify polypharmacological kinase inhibitors[12–15]. Such chemical probes have provided tools for exploring kinase networks and potential leads for therapeutic development. Here, we demonstrate an alternative approach: starting from an already approved clinical kinase inhibitor to retain drug-like properties, we use chemical and genetic modifier screens to rationally improve therapeutic index by evolving compounds towards unique networks of kinase targets.

An unbiased screen of FDA drugs within a *Drosophila* MTC model led us to several KIs that target members of the mitogen-activated protein kinase (MAPK) network, including the structurally similar compounds sorafenib and regorafenib as well as trametinib; a finding that is consistent with studies that the RET oncogene acts via the RAS/RAF/MEK/ERK pathway[16]. Intriguingly, sorafenib has shown promise in human MTC; however, caution has arisen due to adverse effects including rare but fatal toxicity associated with sorafenib treatment[17,18]. We therefore employed chemical and genetic modifier screens to explore the kinase networks modulated by sorafenib, and then used this information to create novel

compounds with unique target profiles and biological activity within whole animals. The result of our approach is a new class of *T*umor-*C*alibrated *I*nhibitors (TCIs) that are 'tuned' to exhibit exceptional efficacy in pre-clinical models of MTC when benchmarked against other tool compounds or FDA-approved MTC drugs.

Results

Sorafenib showed modest effects in a *Drosophila* MTC model

We previously reported a transgenic *Drosophila* model for MTC (*ptc>dRet^{M955T}*) in which the *patched* (*ptc*) promoter directs expression of the M955T isoform of *Drosophila* Ret, designed to model the human oncogenic isoform RET(M918T)[14,16]. 100% of *ptc>dRet^{M955T}* flies died before adulthood when cultured at 25°C. This provided a 'rescue-from-lethality' assay for compounds that suppress oncogenic Ret-dependent lethality during fly development (Supplementary Figs. 1a and 1b)[14], and a quantitative measure of whole animal therapeutic index.

We tested the full panel of KIs approved by the FDA for cancer therapy as of 2016. Of the 31 KIs tested, the MAPK pathway inhibitors sorafenib [**1**], regorafenib [**2**], and trametinib [3] provided the strongest rescue of *ptc>dRet^{M955T}* flies to adulthood, though rescue for each drug was only moderate (Fig. 1a). Sorafenib and regorafenib are structurally related multi-kinase inhibitors, originally developed as RAF inhibitors[19,20]. Trametinib is a highly selective MAPK/ERK kinase 1 and 2 (MEK1/2) inhibitor[21]. Regorafenib is approved for colorectal cancer[20], and sorafenib has previously been demonstrated as effective in human MTC cell lines[22,23], an observation that we confirmed (see below). Due to its reported clinical activity in MTC[17,18,24,25], we focused on sorafenib for exploring targets and mechanisms of RET-based transformation.

In addition to directing late lethality, the *ptc>dRet^{M955T}* transgenes targeted *dRet^{M955T}* expression to a stripe of cells at the midline of the developing wing disc epithelium; targeted cells were visualized with an included *UAS-GFP* transgene. We previously showed that these *ptc>dRet^{M955T}* cells undergo an epithelial-to-mesenchymal transition (EMT) and subsequent basal invasion beneath the wing epithelium, modeling early steps in cell transformation and metastasis[14]. Sorafenib consistently suppressed both EMT and migration of *dRet^{M955T}*-expressing wing cells (Fig. 1b), demonstrating its ability to reduce aspects of transformation.

Despite providing the strongest improvement of fly viability, the penetrance of sorafenib rescue was low (5%) and the therapeutic window was small. This is consistent with reports from human patients: sorafenib displays limited efficacy in treating liver, renal, and differentiated thyroid carcinoma (DTC), and is associated with severe side effects including diarrhea, pancreatic atrophy, and emergent skin tumors[17,18,26–28]. We therefore focused our efforts on defining a new chemical space that better addresses the oncogenic RET network in a whole animal context.

Chemical modifier screens identify improved analogs

Sorafenib inhibits multiple kinases including RET, BRAF, and KDR/VEGFR[19]. Based on structural analysis of sorafenib bound to several of these kinases (Supplementary Fig. 1c), we deconstructed the compound into four subunits: (i) *hinge binder* that occupies the ATP-binding site of a target kinase (held constant in our studies), (ii) *spacer*, (iii) *linker*, and (iv) *cap* (Fig. 2a, left). As part of our chemical modifier screen, we developed a library of sorafenib analogs to be used for structure-activity relationship (SAR) analysis in the *ptc>dRet*^{M955T} model. This series included analogs with varied linkers (L1–L6), spacers (S1–S4), or combinations in the context of four different caps (C1–C4; Fig. 2a, right). For our initial series, the activity of compounds was assessed based on their rescue of *ptc>dRet*^{M955T} animals (Supplementary Fig. 1d).

Several general features and informative SAR emerged from this analysis. For example, in the context of the cap test group (C1–C4), bioisosteres of the urea linker including thiourea, squaramide, and α-amino acetamide, were inactive (0% rescue). All analogs with spacer S4 were also ineffective (0% rescue), whereas compounds with the amide (L2) and sulfonamide (L3) linkers showed weak rescue activity (Supplementary Figs. 1d, 2a, and 2b). The urea (L1) proved most effective with variations at the cap position (Supplementary Fig. 1d).

From our initial series we identified structurally related analogs (LS1-15) [4] and (APS3-69-1) [5] as more effective than sorafenib in rescuing lethality of *ptc>dRet*^{M955T} animals (Fig. 2b); both were as effective as sorafenib in suppressing EMT and invasion (Fig. 2c). In contrast, other close analogs such as (LS1-37) [6] enhanced cell migration indicating that it activated the *dRet*^{M955T} transformation network. **6** proved toxic even when fed to control, non-transformed flies, indicating that it also promoted whole body toxicity (Figs. 2b and 2c).

Comparing efficacy across the library was strongly informative. For example, sorafenib and **4** share a common S1 spacer structure; each was more effective and less toxic than their spacer S2 counterparts regorafenib and **5** respectively. Further, in the context of linker L1, alterations in the cap—the structure that binds to kinases' DFG pocket—was especially useful for tuning compound efficacy in *ptc>dRet*^{M955T} animals. Together, these studies provided a useful entry point by defining a library of structurally related tool compounds that altered Ret-mediated transformation within whole animals. We define these new compounds as 'Tumor Calibrated Inhibitors" or TCIs.

Pro-targets and anti-targets for 4 and sorafenib

To further explore the mechanism of our lead molecules we used a genetic approach to identify kinases that, when partially reduced throughout the developing fly, altered the ability of sorafenib or **4** to suppress *ptc>dRet*^{M955T} lethality (Supplementary Fig. 3a). This genetic approach mimics drug distribution throughout the body. Using temperature to control GAL4 driver activity, we calibrated the viability of *ptc>dRet*^{M955T} flies to ~50% in the presence of **4**. We used this sensitized assay to identify genetically dominant 'pro-targets' and 'anti-targets', genes that when heterozygous increased or decreased rescue, respectively (Supplementary Figs. 3b–h). Pro-targets serve as positive modifiers of TCI

efficacy: increasing inhibitory activity against a pro-target should improve a lead compound's overall therapeutic index. Anti-targets serve as negative modifiers within a drug's network: when inhibited, anti-targets act as liabilities that can reduce a drug's tumor efficacy and/or promote a drug's whole body toxicity. Overall, 199 kinase genes were tested, covering more than 80% of the predicted *Drosophila* kinome (Supplementary Table 1).

For example, **4** rescued *ptc>dRet*^{M955T} to 50% viability at 23°C. Removing a functional allele of *Lk6* (*ptc>dRet*^{M955T},*Lk6*$^{-/+}$) led to 0% survival to adulthood in animals treated with **4** (Fig. 3a); *Lk6*$^{-/+}$ control flies showed nearly 100% survival in a non-*dRet*^{M955T} background (Supplementary Fig. 4a). This defined Lk6 as an 'anti-target' of **4**. Lk6 is the fly ortholog of mammalian MAP kinase interacting serine/threonine kinases 1 and 2 (MKNKs), emerging cancer targets (*e.g.*, refs. 29,30); our work suggests MKNKs may prove a liability as a therapeutic target in at least some contexts. In contrast, treating genotypically *ptc>dRet*^{M955T},*phl*$^{-/+}$ flies with **4** led to 96% viability. The *phl* locus encodes the *Drosophila* ortholog of RAF kinase, defining RAF as a genetic pro-target of **4** (Fig. 3b, Supplementary Tables 2 and 3). Overall, we identified 22 strong pro-target genes in which heterozygosity significantly improved (>91%) animal viability in the presence of **4** feeding (Fig. 3b, Supplementary Table 2, Supplementary Fig. 4b).

We also performed a similar genetic modifier kinome screen with flies fed sorafenib. Remarkably, 17/22 pro-targets for **4** failed to show a similar functional interaction when tested with sorafenib (Supplementary Fig. 4b), indicating different whole animal activities despite similar chemical structures between the two compounds. Further, we identified eight strong anti-targets for **4** and six strong anti-targets for sorafenib; five anti-targets were shared between the two compounds (Supplementary Figs. 4b and 5, Supplementary Table 3).

Interestingly, reducing Lk6/MKNK activity solely within the tumor itself through targeted knockdown (*ptc>[dRet*^{M955T},*Lk6*^{shRNA}*]*) rescued viability (Supplementary Fig. 6a), the opposite effect of whole animal Lk6 reduction. This suggests that Lk6 acts as a pro-target within the tumor but an anti-target in the context of the animal (Supplementary Fig. 6b), an example of the utility of whole body studies. Some pro-targets and anti-targets also proved to be "dominant genetic modifiers" that altered survival of *ptc>dRet*^{M955T} animals in the absence of drug (denoted by asterisks in Supplementary Tables 2 and 3), suggesting they directly regulate the *dRet*^{M955T} transformation network. Overall, our chemical genetic studies provided a whole animal roadmap to further improve TCI efficacy.

Developing the novel TCIs APS5-16-2 and APS6-45

The genetic screens with sorafenib and **4** provided functional data for kinase inhibitory activities that we could enhance (pro-targets) or reduce (anti-targets) to improve the therapeutic index of TCIs. Based on our SAR studies and genetic identification of key pro-targets and anti-targets, we hypothesized that overall TCI therapeutic index would be improved by further modifications on the cap group, the chemical domain that directly binds the DFG-out pocket of target kinases and for which we observed compelling SAR in our initial TCI series.

For example, removing a single fluorine (**7**; APS4-54) or all fluorines (**8**; APS4-35-1) from the $–CF_3$ of **4**'s cap structure resulted in reduced rescue of *ptc>dRet*^{M955T} viability (Fig. 4a; discussed in Online Methods). In computational analysis of binding pocket sizes, we found the cap-binding element in kinases (*i.e.* the DFG-out sub-pocket) differs in composition and size between kinases[31]. For example, we calculated estimated sizes for the DFG-out sub-pocket in RET and BRAF as approximately 163 $Å^3$ and 136 $Å^3$, respectively (Fig. 4b).

We hypothesized that reducing the size of the cap structure was increasing binding to putative anti-targets, in turn reducing TCI efficacy. We therefore examined our ability to selectively remove anti-target activity from the TCIs by enlarging the cap's 5-position $–CF_3$ group. For this, we focused on perfluoroalkyl substitution patterns at the $–CF_3$ position to increase the size, complexity, and target profile of the TCI compounds. To the best of our knowledge, extended perfluoroalkyl group analogs of sorafenib have not been previously synthesized.

Expanding **4**'s cap group by substituting $–CF_3$ with a $–C_2F_5$ or $–iso C_3F_7$ generated the compounds APS5-16-2 [**9**] and APS6-45 [**10**], respectively (Fig. 4a, Supplementary Fig. 6c). Oral administration of **9** and especially **10** strongly improved overall *ptc>dRet*^{M955T} adult survival beyond **4** at optimal doses; **10** rescued *ptc>dRet*^{M955T} flies to a remarkable 84% overall viability (Fig. 4a, Supplementary Figs. 2a and 2b). This level of rescue is higher than all previously tested compounds including our previously reported compound AD80 (Supplementary Fig. 2b)[14]. The therapeutic window of **10** was broader and included lower doses than sorafenib or **4** (Supplementary Fig. 2b). Of note and inconsistent with simply increasing lipophilicity (*i.e.* logP), the straight-chain $–C_3F_7$ and $–C_4F_9$ analogs were markedly reduced in their ability to rescue viability of *ptc>dRet*^{M955T} flies (Supplementary Fig. 6d). We conclude that—consistent with our genetic, computational, and initial SAR studies—expanding the cap structure improved overall TCI therapeutic index.

APS6-45 acts through multiple mechanisms

To better understand the improvements in activity of **9** and **10** relative to the FDA drugs that we started with, we utilized pharmacodynamic markers of pro-target and anti-target signaling within the fly. For example, the MKNK ortholog Lk6 proved an especially strong anti-target of both sorafenib and **4** (Supplementary Fig. 4b and 5, Supplementary Table 3). Previous work has linked Lk6 to suppression of RAS pathway activity in *Drosophila*[32]. Consistent with this view, *765>dRet*^{M955T}*,Lk6*$^{-/+}$ flies showed strongly enhanced wing venation and poor wing structure—validated *in vivo* readouts of RAS pathway activity[33]—compared to *765>dRet*^{M955T} control flies (Fig. 5a, left). These wing defects were suppressed by the selective RAS pathway inhibitor trametinib (Fig. 5a, right), confirming that MKNK/Lk6 is acting as a repressor of RAS pathway activity (Supplementary Fig. 6b).

Our analysis of experimentally determined structures and homology models of the MKNK family member MKNK1 indicated that its allosteric DFG-pocket was slightly smaller than that of RET, an estimated 150 $Å^3$ (Fig. 4b). Indeed, while **10** exhibited only a small decrease in *in vitro* MKNK1 binding relative to sorafenib, **9** exhibited significantly reduced MKNK1 binding (Fig. 5b). Our *in vivo* data matched these measured activities. Reducing *Lk6*

(*ptc>dRet*^{M955T}*,Lk6*$^{-/+}$) reversed suppression of *ptc>dRet*^{M955T} cell migration by sorafenib or **4** (Fig. 5c), consistent with Lk6 acting as an anti-target to both compounds. In contrast, efficacy of **9** and **10** were not affected by reduced *Lk6* (Fig. 5c), consistent with their lower binding to MKNK1.

To validate the effects of **10** on RAS/MAPK signaling, we used fly eye tissue morphology as a readout. Targeted expression of either *dRas*^{G12V} or *dRet*^{M955T} in the developing eye epithelium lead to aspects of transformation, generating a 'rough eye' phenotype[32,34]. Dissecting dying (vehicle-treated) *ptc>dRet*^{M955T} mature pupae, we observed a rough eye phenotype in the anterior-most region of the eye (Fig. 5d), consistent with expression of *ptc* within the anterior eye field[35]. **10** strongly suppressed this anterior rough eye phenotype both in pupae and in rescued adults; other TCIs and AD80 did not (Fig. 5d). These results further indicate that **10** strongly inhibits Ret-mediated transformation with minimal whole animal toxicity.

RAF is both pro-target and pharmacological anti-target

In the course of our genetic studies one kinase, RAF, proved to have both pro-target and anti-target properties. The RAS/RAF/MAPK pathway plays a key role in mediating RET-induced transformation, as further emphasized by our genetic screens (Fig. 3b, Supplementary Fig. 5) and by *ptc>dRet*^{M955T} rescue by trametinib (Fig. 1a; ref. 36). Recent studies have demonstrated that first generation BRAF inhibitors can activate BRAF dimers at low doses through “inhibitor-induced transactivation”: drug-bound RAF protomers stimulate the kinase activity of drug-free RAF protomers, leading to activation of downstream MAPK activity[37,38]. Higher drug doses are required to reduce the number of drug-free RAF protomers and therefore BRAF/MAPK activity.

Sorafenib was originally developed as a RAF inhibitor of relatively modest binding activity[39], raising the possibility that sorafenib and some TCIs direct a similar low dose activation/high dose inhibition response in our *Drosophila* platform. We again used wing venation in the adult fly to explore TCI dose effects on RAS/MAPK pathway activity. Low dose (10 μM final food concentration) feeding of *765>dRet*^{M955T} larvae with sorafenib or **4** stimulated significant excess wing vein material compared to no-drug controls; this wing venation was strongly suppressed with co-feeding of trametinib (Figs. 6a and 6b). In contrast, higher doses of sorafenib or **4** that successfully rescued *ptc>dRet*^{M955T} viability did not promote ectopic wing venation in *765>dRet*^{M955T} flies (Figs. 6a and 6b). This bell-shaped dose curve—intermediate doses of sorafenib or **4** directed increased wing venation—is consistent with the inhibitor-induced transactivation model.

Our calculations predicted that the substitutions at the caps’ 5-position of **9** and **10** could cause a steric clash with BRAF’s DFG-pocket (Fig. 4b). Indeed, our cell-free *in vitro* studies indicated reduced BRAF binding by **9** and **10** when compared to sorafenib and **4** (Fig. 5b, Supplementary Dataset 1). Further, the ability of **10** to transactivate BRAF required ~30-fold higher drug concentrations relative to sorafenib in two cancer cell lines (Supplementary Figs. 7a and 8). *In vivo*, both **9** and **10** failed to promote ectopic wing venation in

765>dRet^{M955T} flies at any dose (Fig. 6b), reflecting a reduced ability to directly transactivate RAF dimers *in vivo*.

While targeting RAF kinases has shown clinical success, our results suggest the interesting possibility that at least some kinase inhibitors could exhibit a broader therapeutic window if RAF kinases were removed as targets. That is, in some contexts RAF may serve as a pro-target but also a pharmacological anti-target.

APS6-45 suppressed growth of human MTC cells

10 strongly inhibited RAS pathway signaling in human MTC cell lines TT and MZ-CRC-1 (Supplementary Fig. 7b). Furthermore, **9** and especially **10** strongly suppressed colony formation of TT cells in soft agar when compared with sorafenib and **4** (Fig. 6c). To characterize **10** in the mouse, we first measured maximum tolerated dose (MTD) and multiple pharmacokinetic (PK) parameters. Oral dosing of **10** did not cause detectable toxic effects at a single dose of 160 mg/kg; of note, one-eighth of this dose (20 mg/kg p.o.) reached a concentration of approximately 10 μM in blood plasma (Supplementary Fig. 7c). **10** also demonstrated a relatively long half-life (5.6 hours) and overall PK parameters similar to sorafenib[40]. These measurements suggest that **10** has retained drug-like properties.

Strikingly, administration of **10** inhibited growth of established TT tumors in the subcutaneous tissue of xenografted nude mice far more potently than sorafenib or cabozantinib, a kinase inhibitor FDA-approved for MTC[41]. Overall, **10** treatment led to partial or complete responses in 75% of dosed mice (Figs. 6d and 6e). Importantly, **10** did not affect body weight of dosed mice after 30 days, demonstrating *in vivo* safety (Fig. 6f). Our animal experiments collectively indicate that, at least with respect to MTC, **10** is a highly efficacious lead with favorable *in vivo* properties.

Discussion

In this paper, we demonstrate a whole animal platform that combines *Drosophila* genetics with medicinal chemistry to develop novel compounds from FDA-approved drugs in a rational, stepwise manner. We focused on sorafenib as a clinically important cancer therapeutic that nonetheless has demonstrated significant contraindications in the clinics (*e.g.*, refs. 26,42).

We demonstrate two steps in which the target profile of sorafenib was tuned for greater therapeutic index within preclinical models of MTC (Supplementary Fig. 9a). In the first step, SAR studies identified a correlation between the size and complexity of the cap group structure within our early analog series and whole animal rescue activity. In the second step, we identified pro-targets and anti-targets that established a map of chemical genetic interactions. Based on (i) specific trends in our SAR series and (ii) correlated homology modeling of the allosteric pocket in the DFG-out conformation of pro-targets and anti-targets, we expanded a substituent of the cap structure. The result was reduced activity against anti-target kinases (*e.g.*, MKNKs) coupled with strongly improved whole animal efficacy (Supplementary Fig. 9b).

Intriguingly, TCI efficacy did not simply track with activity against RET: for example, **10** showed much stronger efficacy relative to sorafenib but weaker RET binding (Fig. 5b, Supplementary Table 4). Supplementing activity against RET, our data indicates that several pro-targets and anti-targets likely contribute to TCIs' overall network effect (Supplementary Fig. 10; Supplementary Dataset 1). We provide evidence that activity against MKNK and RAF kinases limited the level to which sorafenib and several TCIs could be improved, despite the clear importance of these kinases in tumor growth and development. Together, our data suggests that MKNKs, mTOR, eIF-4E, and their translational targets constitute an 'anti-target' pathway cassette in RET-dependent cancers specifically in the context of the whole body (Supplementary Fig. 6b). Consistent with this hypothesis, MKNK binds to mTOR to sustain mTORC1 activity[45].

Potential caveats of our approach include species-specific differences in *Drosophila* and mammalian kinases as well as differences in drug metabolism. Notwithstanding, the drug-like properties of **10** is supported by PK, MTD, and mouse xenograft data. We note that the whole animal platform that guided SAR was instrumental in working towards the $–C_2F_5$ and $–iso C_3F_7$ modifications; more standard screening platforms including biochemical and cell line-based RET inhibition assays would have led us towards different compounds.

In our current study we used fluorine-based cap modifications to alter kinase specificity through the DFG-out pocket of target kinases. The potential of modifying existing drugs based on harnessing the unique properties of fluorine is a burgeoning area of investigation[46,47], with a growing list of known drugs that vary in fluorine substitutions in clinical use including enzalutamide (4 fluorines), fulvestrant (5 fluorines), and aprepitant (7 fluorines). Indeed, the importance of fluorines in pharmacology and drug design[48] suggests the potential for systematic perfluoroalkyl group substitutions as a potential route towards unique chemical and target space.

In recent years, an important development in cancer has been the move towards precision therapeutics in which the focus is typically a single target. Here, we provide an alternative, complementary approach: an efficient, inexpensive platform for generating polypharmacological drugs that are optimized for kinase networks both within the tumor and in the context of the whole animal. We identify multiple kinase activities that strongly impact pharmacological responses, and demonstrate how this approach can be used for tuning drugs into new and potentially useful therapeutic spaces. Our approach may also prove useful in drug development strategies outside of oncology, including neural and cardiovascular diseases, where systemic or chronic treatment requires accounting for whole body networks and where drug discovery can prove both challenging and expensive.

Online Methods

Fly stocks

Kinase-mutated, shRNA, and balancer fly stocks were obtained from Bloomington *Drosophila* Stock Center (BDSC; Bloomington, IN). To prepare kinase-mutated stocks to be used in genetic screening (Supplementary Table 1), *FM6*-, *FM7a*- *FM7c*- or *FM7i*-balanced flies with mutated kinase genes on the X chromosome were outcrossed with *FM7c-Tb-RFP*-

balanced flies, and *CyO-, SM5-*, or *SM6a*-balanced flies were rebalanced with *CyO-Tb-RFP* balancer[50]. Likewise, *TM3-, TM6C-*, or *MKRS*-balanced flies were rebalanced with *TM6B* balancer containing *Tb*. The active mutant form of *dRet* (*dRet*^{M955T}) carries M955T mutation which corresponds to M918T mutation commonly reported for multiple endocrine neoplasia (MEN) type 2B patients[12,14,16,34]. The *ptc-gal4,UAS-GFP;UAS-dRet*^{M955T}/*SM5*$^{tub-gal80}$*-TM6B* and *UAS-dRet*^{M955T};*765-gal4*/*SM5*$^{tub-gal80}$*-TM6B* transgenic flies were prepared according to standard protocols, and crossed with w^{-} and kinase-mutant flies for drug screening and kinome genetic screening, respectively (Supplementary Figs. 1b and 3b–h). To validate the results of genetic screening, we also randomly picked and tested ten more alleles for the pro-targets, and obtained essentially similar results for nine genes, confirming the integrity of our experimental design to determine pro-targets.

Fly assays

FDA-approved drugs and TCIs were purchased from Selleck Chemicals (Houston, TX), LC Laboratories (Woburn, MA), and Tocris Bioscience (UK), or synthesized in-house. AD80 was synthesized as previously described[14]. All compounds were dissolved in DMSO (Sigma-Aldrich; St. Louis, MO) and mixed with semi-defined fly medium (BDSC) to make drug food (0.1% final DMSO concentration). *ptc>dRet*^{M955T} embryos with or without kinase heterozygous mutations were raised until adulthood on drug food for 15 days at 23°C (genetic screening) or 13 days at 25°C (drug screening and wing venation and rough eye assays). The number of empty pupal cases (*A* in Supplementary Fig. 1a) was divided by that of total pupal cases (*P*) to determine % viability. Small molecule screening information are summarized in Supplementary Table 5. Fly randomization was used throughout the assays.

Cell migration and wing venation assays

For *in vivo* cell migration assays, third-instar larvae were dissected to collect developing wing discs. After fixation with 4% paraformaldehyde in PBS, discs were whole-mounted and observed for *dRet*^{M955T}-expressing cells labeled with GFP under a confocal microscope. Phospho-Src was stained with rabbit anti-Src(pY418) antibody (#44-660G, Thermo Fisher Scientific; Waltham, MA). For wing venation assays, *UAS-dRet*^{M955T};*765-gal4*/*SM5*$^{tub-gal80}$*-TM6B* transgenic flies were crossed with either w^{-} or *Lk6*$^{-/+}$ flies to generate *765>dRet*^{M955T} or *765>dRet*^{M955T}*,Lk6*$^{-/+}$ flies, respectively. Their progenies were raised in the presence or absence of compounds, and adult wings were scored for abnormal wing venation. Investigators were blinded to group allocations.

Soft agar assay

TT human MTC cells (ATCC; Manassas, VA) were cultured in 0.3% agar according to the standard protocol in the presence or absence of TCIs for three weeks. The number of growing colonies was divided by that of seeded cells to calculate colony formation efficiency.

Kinase percent Inhibition measurements

TCIs were assayed against a panel of purified human kinases (Thermo Fisher Scientific) to measure percentage inhibition values and derive kinome profiles (Supplementary Table 4).

All compounds were screened at 1 μM, using two experimental replicates to determine percent inhibition values. Detailed procedures for kinase reactions and assay formats are described at http://www.thermofisher.com/kinaseprofiling.

Kd measurements

Kd values and single point screens were determined by DiscoverX (Fremont, CA) using a bead based competition assay (KINOMEscan). In brief, kinases are expressed on phage and immobilized on beads via active site-directed ligands. Test compounds are premixed with kinases and assayed for the ability to compete for immobilized ligands. Binding constants are calculated with a standard dose-response curve and the Hill equation, with Hill slope set to -1. The method has been used extensively to characterize kinase inhibitor-binding data[10]. For each TCI-kinase pair, an 11-point series ranging from 30,000 to 0.5 nM, in 3-fold dilutions, were used to derive Kd values. Kd values are the average of two experimental replicates.

RAF transactivation assays in human cancer cell lines

HCT-116 and LOVO cells (ATCC) were maintained in DMEM or DMEM/F12 respectively supplemented with antibiotics, 10% FBS, and 2 mM glutamine. Cells were seeded in 100 mm plates for assays. After 24 hours, cells were treated with **1** or **10** for 1 hour. Cells were then harvested in PBS and lysed in buffer (50 mM Tris pH 7.4, 150 mM NaCl, 1% NP-40, 0.5% Sodium Cholate, 0.1% SDS) containing protease and phosphatase inhibitors (Thermo Fisher Scientific). Cell lysates were spun at 20,000 rpm for 20 min and supernatants were extracted, normalized for total protein based on the BCA assay (Thermo Fisher Scientific), and mixed with 6× SDS dye prior to application to a 4–15% Tris-HCl gradient gels. Following PAGE separation, samples were transferred to nitrocellulose and blotted for the indicated proteins using antibodies for pMEK (#9154), pERK1/2 (#9101), and total MEK (#8727) (all from Cell Signaling Technology; Danvers, MA).

Signaling pathway activity analysis

TT and MZ-CRC-1 human MTC cells were treated with either vehicle (0.1% DMSO), **1** (1 μM), or **10** (1 μM). After 1 hour, cells were harvested and analyzed for activities of Ras pathway effectors by western blotting using antibodies against pMEK (#9154), total MEK (#8727), pERK1/2 (#9101), total ERK1/2 (#4695), and pS6 (#4858) (all from Cell Signaling Technology).

Dosing experiments in mice

Toleration assays for **10** were performed by Washington Biotechnology (Baltimore, MD). Briefly, five female athymic nude mice (6 weeks) were administered with increasing oral doses of **10** starting at 0.1 mg/kg/day and observed for 2 days for signs of clinical distress such as weight loss, discharges, and morbidity. Dose was gradually escalated up to 160 mg/kg/day, and no such signs were observed.

Phamacokinetics assays for **10** were performed by Medicilon Preclinical Research (Shanghai, China). Twenty mg/kg of **10** was dosed orally to male ICR mice (6 weeks of

age), and its plasma concentrations were determined at 0.25, 0.5, 1, 2, 4, 8, 10, and 24 hours post dosing. No treatment-related clinical signs were observed following dosing.

Xenograft assays were also performed by Washington Biotechnology. Forty female nude mice (6 weeks) were implanted subcutaneously with TT cells. When tumor volume achieved ~120 mm^3, mice were randomly grouped into four arms, and each arm was dosed p.o. five days per week with vehicle (Cremophor EL/ethanol (1:1) diluted 4-fold with water) or 10 mg/kg/day of cabozantinib (LC Laboratories), **1** (LC Laboratories), or **10**. These doses were expected to give clinically relevant AUCs and maximum plasma concentrations of each drug[40,41,51–53].

All mouse experiments were carried out according to guidelines set forth by American Association for Accreditation of Laboratory Animal Science (AAALAC) or the Office for Laboratory and Animal Welfare (OLAW) division of the National Institute of Health (NIH).

Statistics

Two-sided Student's *t*-tests were performed using PRISM (GraphPad Software, Inc.; La Jolla, CA). Sample numbers in each experiment are summarized in Supplementary Dataset 2. Fly assays and soft agar assay were repeated twice. Small molecule screening data are included in Supplementary Table 5.

Computation: DFG-out modeling

1 and other related kinase inhibitors are known type-II inhibitors that bind the DFG-out conformation, and we hypothesized that the TCIs were also type-II kinase inhibitors. To dock type-II inhibitors we used atomic structures of pro-targets and anti-targets in their DFG-out conformation. Some of our pro-targets/anti-targets did not have known structures in the DFG-out conformation, and we used homology modeling to predict their structures. In particular, we used DFGmodel, a pipeline for generating DFG-out models from the DFG-in structure or sequence information alone[31]. We have previously shown that models generated by DFGmodel are highly accurate using various assessment measures such as RMSD and TM-Score, and can enrich for known type-II inhibitors among other molecules within diverse chemical libraries.

Briefly, the sequence of the target kinases were aligned to a set of template kinase structures that represent a unique range of DFG-out conformations. DFGmodel then utilized the automatic multi-template function of MODELLER[54] to generate homology models of the DFG-out conformation. Fifty initial models were built for each alignment and ranked according to the inhibitor-binding site volume calculated by POVME 2.0[55]. To address the flexibility in the binding site, the average volume of the DFG-pocket, resided in the inhibitor-binding site, was calculated to select the 10 models with the largest binding site volume. This model selection was shown to correlate with the ability of DFG-out models to discriminate known type-II inhibitors from non-binders thereby optimizing the model for protein-type II inhibitor complementarity[31]. For the DFG-out models of RET, BRAF, and MKNK1, we estimated the size of their respective DFG-out sub pockets as 163 $Å^3$, 136 $Å^3$, and 150 Å (Fig. 4b).

Computation: Molecular docking

The ligand poses were pre-generated with Openeye (http://www.openeye.com) OMEGA 2.5.1.4 (OpenEye Scientific Software, Santa Fe, NM) using the default settings. For each molecule, an ensemble of a maximum of 300 conformers with reasonable internal energy was generated. Each conformer was then docked against an ensemble of 10 DFG-out models for each kinase using OpenEye FRED 3.0.1 (OEDocking 3.0.1: OpenEye Scientific Software; ref. 56), which uses a Gaussian-based scoring function (default settings). Top-scoring ligand poses from the ensemble of models were selected for visual inspection to eliminate poses with strained ligand conformations. We prioritized poses that make favorable interactions such as polar interactions with the kinase hinge region and the conserved **α**C-helix glutamate residue.

Computation: Torsion angle

The torsional energy of the urea linker to the N-substituents was calculated with Schrödinger's 2017-01 Maestro (version 11.2, Schrödinger, LLC, New York, NY, 2015) using the molecular mechanics OPLS3 force field[57]. To mimic the environment of protein interior (dielectric constant **ε** ~ 6–7; ref. 58), we used chloroform (**ε** ~ 5) as solvent. The torsion angles were scanned at two-degree intervals. The relative torsional energy was converted to population size based on the Boltzmann distribution equation and was plotted against the torsion angles. The population landscape plot was compared to the corresponding torsional angles observed in the reference **1** x-ray structures.

Chemistry Methods and Spectra

For all chemistry methods and spectra for intermediates and final compounds, please see Synthetic Methods and Compound Characterization included in Supplementary Note.

Computational analysis of TCIs suggest a favorable ligand conformation

In our SAR studies we noted that subtle structural changes in the TCIs' cap groups led to especially strong differences in rescue from dRet^{M955T}-driven lethality. To better understand our observed SAR, we explored the physical features of these cap structures *in silico*, looking for correlations between structure and whole animal function (Fig. 2). Several cap properties did not significantly correlate with efficacy including partial charge distribution, pKa, clogP, and molecular dipole.

We did, however, observe correlation between TCIs' efficacy and the forcefield-based calculated torsional energy (FCTE) of their N-substituted linker (urea)-cap (*i.e.*, the preferred angle between cap and linker; Supplementary Fig. 11). **1**'s cap requires rotation to a *cis* conformation to bind target kinases' allosteric pocket: FCTE values are in agreement with the optimal torsion angle (~158°) between linker and cap observed in crystal structures of bound **1** (*e.g.*, PDB ID: 1UWH). In the unbound state, FCTE indicated **1** does not have a strong conformational preference between *cis* and *trans*; suggesting its cap may therefore align itself into the *cis* conformation to permit proper kinase binding. Therefore, placing a fluorine atom at the cap's 2-position would be expected to constrain **4**'s cap to the more optimal *cis* binding conformation even in the unbound state due to (i) repulsive interaction

with the linker's urea oxygen and (ii) favorable multipolar interaction with the linker's urea hydrogen.

Constraining **4**'s cap into the *cis* conformation more closely matches the bound-state conformation of **1** reported for kinase co-crystal structures (Supplementary Figs. 1c and 11), suggesting optimized binding towards kinases as opposed to enhanced activity on possible off-targets in different protein classes. Consistent with the importance of 'constraining' the cap structure into the *cis* conformation, removal of the 2-fluoro group in **4** reduced survival (LS1-11-2 [**e**]; Supplementary Figs. 2a and 2b). That is, constraining **4**'s unbound-state conformation to 'pre-match' its optimal kinase binding conformation correlated with a strong improvement in whole animal efficacy.

However, ligand conformational dynamics and predicted kinase-ligand interactions alone were limited in providing guidelines for further improving our lead compounds. For example, APS4-54 [**7** or **i**] and APS4-35-1 [**8**] displayed poor whole animal activity relative to **4** despite similarly constrained torsion angle dynamics (Fig. 4a, Supplementary Figs. 2a and 2b). The current limitations of our computationally predicted kinase-ligand interactions could be aided through experimental data; for example, the use of X-ray crystal structures over homology models. The incorporation of such methods could enhance the overall platform and our ability to predict novel compounds.

Supplementary Material

Refer to Web version on PubMed Central for supplementary material.

Acknowledgments

We thank K. Shokat, B. DeVita, and M. Birtwistle for critical comments on the manuscript. We thank members of the Cagan, Dar, and Schlessinger laboratories for important discussions. We thank Peter Smibert for *ptc>dRet*^{M955T} flies, Kevin Cook and the Bloomington Drosophila Stock Center for kinome mutant fly lines. M.S. was supported by The Kyoto University Young Scholars Overseas Visit Program. M.S. and R.C. were supported by NIH grants U54OD020353, R01-CA170495, and R01-CA109730 and DOD grant W81XWH-15-1-0111. P.M.U.U. and A.S. were supported by NIH grant R01-GM108911, and also by Department of Defense grant W81XWH-15-1-0539 (A.S.). The Dar laboratory is supported by Innovation awards from the NIH (DP2 CA186570-01) and Damon Runyon-Rachleff Foundation. A.C.D. is a Pew-Stewart Scholar in Cancer Research and Young Investigator of the Pershing-Square Sohn Cancer Research Alliance. We thank OpenEye Scientific Software, Inc. for granting us access to its high-performance molecular modeling applications through its academic license program. This work was also supported by Scientific Computing at the Icahn School of Medicine at Mount Sinai and NCI grant P30 CA196521 to the Tisch Cancer Institute. The data and reagents that support the findings of this study, including fly lines, homology models, and compounds, are available from the corresponding authors upon request.

References

1. Druker BJ, et al. Efficacy and safety of a specific inhibitor of the BCR-ABL tyrosine kinase in chronic myeloid leukemia. N. Engl. J. Med. 2001; 344:1031–1037. [PubMed: 11287972]
2. Flaherty KT, et al. Inhibition of mutated, activated BRAF in metastatic melanoma. N. Engl. J. Med. 2010; 363:809–819. [PubMed: 20818844]
3. Hollingsworth SJ. Precision medicine in oncology drug development: a pharma perspective. Drug Discov. Today. 2015; 20:1455–1463. [PubMed: 26482740]
4. Kandoth C, et al. Mutational landscape and significance across 12 major cancer types. Nature. 2013; 502:333–339. [PubMed: 24132290]

5. Lawrence MS, et al. Discovery and saturation analysis of cancer genes across 21 tumour types. Nature. 2014; 505:495–501. [PubMed: 24390350]
6. Hay M, Thomas DW, Craighead JL, Economides C, Rosenthal J. Clinical development success rates for investigational drugs. Nat. Biotechnol. 2014; 32:40–51. [PubMed: 24406927]
7. Meanwell NA. Improving drug candidates by design: a focus on physicochemical properties as a means of improving compound disposition and safety. Chem. Res. Toxicol. 2011; 24:1420–1456. [PubMed: 21790149]
8. Knight ZA, Lin H, Shokat KM. Targeting the cancer kinome through polypharmacology. Nat. Rev. Cancer. 2010; 10:130–137. [PubMed: 20094047]
9. Fleuren EDG, Zhang L, Wu J, Daly RJ. The kinome 'at large' in cancer. Nat. Rev. Cancer. 2016; 16:83–98. [PubMed: 26822576]
10. Davis MI, et al. Comprehensive analysis of kinase inhibitor selectivity. Nat. Biotechnol. 2011; 29:1046–1051. [PubMed: 22037378]
11. Anastassiadis T, Deacon SW, Devarajan K, Ma H, Peterson JR. Comprehensive assay of kinase catalytic activity reveals features of kinase inhibitor selectivity. Nat. Biotechnol. 2011; 29:1039–1045. [PubMed: 22037377]
12. Vidal M, Wells S, Ryan A, Cagan R. ZD6474 suppresses oncogenic RET isoforms in a Drosophila model for type 2 multiple endocrine neoplasia syndromes and papillary thyroid carcinoma. Cancer Res. 2005; 65:3538–3541. [PubMed: 15867345]
13. Wells SA Jr, et al. Vandetanib in patients with locally advanced or metastatic medullary thyroid cancer: a randomized, double-blind phase III trial. J. Clin. Oncol. 2012; 30:134–141. [PubMed: 22025146]
14. Dar AC, Das TK, Shokat KM, Cagan RL. Chemical genetic discovery of targets and anti-targets for cancer polypharmacology. Nature. 2012; 486:80–84. [PubMed: 22678283]
15. Sonoshita M, Cagan RL. Modeling Human Cancers in Drosophila. Curr. Top. Dev. Biol. 2017; 121:287–309. [PubMed: 28057303]
16. Mulligan LM. RET revisited: expanding the oncogenic portfolio. Nat. Rev. Cancer. 2014; 14:173–186. [PubMed: 24561444]
17. Lam ET, et al. Phase II clinical trial of sorafenib in metastatic medullary thyroid cancer. J. Clin. Oncol. 2010; 28:2323–2330. [PubMed: 20368568]
18. Ahmed M, et al. Analysis of the efficacy and toxicity of sorafenib in thyroid cancer: a phase II study in a UK based population. Eur. J. Endocrinol. 2011; 165:315–322. [PubMed: 21566072]
19. Wilhelm SM, et al. BAY 43-9006 exhibits broad spectrum oral antitumor activity and targets the RAF/MEK/ERK pathway and receptor tyrosine kinases involved in tumor progression and angiogenesis. Cancer Res. 2004; 64:7099–7109. [PubMed: 15466206]
20. Wilhelm SM, et al. Regorafenib (BAY 73-4506): a new oral multikinase inhibitor of angiogenic, stromal and oncogenic receptor tyrosine kinases with potent preclinical antitumor activity. Int. J. Cancer. 2011; 129:245–255. [PubMed: 21170960]
21. Gilmartin AG, et al. GSK1120212 (JTP-74057) is an inhibitor of MEK activity and activation with favorable pharmacokinetic properties for sustained in vivo pathway inhibition. Clin. Cancer Res. 2011; 17:989–1000. [PubMed: 21245089]
22. Carlomagno F, et al. BAY 43-9006 inhibition of oncogenic RET mutants. J. Natl. Cancer Inst. 2006; 98:326–334. [PubMed: 16507829]
23. Koh YW, et al. Sorafenib and Mek inhibition is synergistic in medullary thyroid carcinoma in vitro. Endocr. Relat. Cancer. 2012; 19:29–38. [PubMed: 22109971]
24. de Castroneves LA, et al. Sorafenib for the Treatment of Progressive Metastatic Medullary Thyroid Cancer: Efficacy and Safety Analysis. Thyroid. 2016; 26:414–419. [PubMed: 26701095]
25. Capdevila J, et al. Sorafenib in metastatic thyroid cancer. Endocr. Relat. Cancer. 2012; 19:209–216. [PubMed: 22285864]
26. Hescot S, Vignaux O, Goldwasser F. Pancreatic atrophy--a new late toxic effect of sorafenib. N. Engl. J. Med. 2013; 369:1475–1476. [PubMed: 24106956]

27. Brose MS, et al. Sorafenib in radioactive iodine-refractory, locally advanced or metastatic differentiated thyroid cancer: a randomised, double-blind, phase 3 trial. Lancet. 2014; 384:319–328. [PubMed: 24768112]
28. Fathi AT, et al. Extensive Squamous Cell Carcinoma of the Skin Related to Use of Sorafenib for Treatment of FLT3-Mutant Acute Myeloid Leukemia. J. Clin. Oncol. 2016; 34:e70–2. [PubMed: 25024084]
29. Teo T, et al. An integrated approach for discovery of highly potent and selective Mnk inhibitors: Screening, synthesis and SAR analysis. Eur. J. Med. Chem. 2015; 103:539–550. [PubMed: 26408454]
30. Basnet SKC, et al. Identification of a Highly Conserved Allosteric Binding Site on Mnk1 and Mnk2. Mol. Pharmacol. 2015; 88:935–948. [PubMed: 26268528]
31. Ung PM, Schlessinger A. DFGmodel: predicting protein kinase structures in inactive states for structure-based discovery of type-II inhibitors. ACS Chem. Biol. 2015; 10:269–278. [PubMed: 25420233]
32. Huang AM, Rubin GM. A misexpression screen identifies genes that can modulate RAS1 pathway signaling in Drosophila melanogaster. Genetics. 2000; 156:1219–1230. [PubMed: 11063696]
33. Karim FD, Rubin GM. Ectopic expression of activated Ras1 induces hyperplastic growth and increased cell death in Drosophila imaginal tissues. Development. 1998; 125:1–9. [PubMed: 9389658]
34. Read RD, et al. A Drosophila model of multiple endocrine neoplasia type 2. Genetics. 2005; 171:1057–1081. [PubMed: 15965261]
35. Shyamala BV, Bhat KM. A positive role for patched-smoothened signaling in promoting cell proliferation during normal head development in Drosophila. Development. 2002; 129:1839–1847. [PubMed: 11934850]
36. Slack C, et al. The Ras-Erk-ETS-Signaling Pathway Is a Drug Target for Longevity. Cell. 2015; 162:72–83. [PubMed: 26119340]
37. Hatzivassiliou G, et al. RAF inhibitors prime wild-type RAF to activate the MAPK pathway and enhance growth. Nature. 2010; 464:431–435. [PubMed: 20130576]
38. Poulikakos PI, Zhang C, Bollag G, Shokat KM, Rosen N. RAF inhibitors transactivate RAF dimers and ERK signalling in cells with wild-type BRAF. Nature. 2010; 464:427–430. [PubMed: 20179705]
39. Lyons JF, Wilhelm S, Hibner B, Bollag G. Discovery of a novel Raf kinase inhibitor. Endocr. Relat. Cancer. 2001; 8:219–225. [PubMed: 11566613]
40. Zarrinkar PP, et al. AC220 is a uniquely potent and selective inhibitor of FLT3 for the treatment of acute myeloid leukemia (AML). Blood. 2009; 114:2984–2992. [PubMed: 19654408]
41. Lacy SA, Miles DR, Nguyen LT. Clinical Pharmacokinetics and Pharmacodynamics of Cabozantinib. Clin. Pharmacokinet. 2017; 56:477–491. [PubMed: 27734291]
42. Zhang L, Zhou Q, Ma L, Wu Z, Wang Y. Meta-analysis of dermatological toxicities associated with sorafenib. Clin. Exp. Dermatol. 2011; 36:344–350. [PubMed: 21507035]
43. Arquier N, Bourouis M, Colombani J, Léopold P. Drosophila Lk6 kinase controls phosphorylation of eukaryotic translation initiation factor 4E and promotes normal growth and development. Curr. Biol. 2005; 15:19–23. [PubMed: 15649359]
44. Joshi S, Platanias LC. Mnk kinase pathway: Cellular functions and biological outcomes. World J. Biol. Chem. 2014; 5:321–333. [PubMed: 25225600]
45. Brown MC, Gromeier M. MNK Controls mTORC1:Substrate Association through Regulation of TELO2 Binding with mTORC1. Cell Rep. 2017; 18:1444–1457. [PubMed: 28178522]
46. Müller K, Faeh C, Diederich F. Fluorine in pharmaceuticals: looking beyond intuition. Science. 2007; 317:1881–1886. [PubMed: 17901324]
47. Curran DP. Chemistry. Fluorous tags unstick messy chemical biology problems. Science. 2008; 321:1645–1646. [PubMed: 18801990]
48. Gillis EP, Eastman KJ, Hill MD, Donnelly DJ, Meanwell NA. Applications of Fluorine in Medicinal Chemistry. J. Med. Chem. 2015; 58:8315–8359. [PubMed: 26200936]

49. Eisenhauer EA, et al. New response evaluation criteria in solid tumours: revised RECIST guideline (version 1.1). Eur. J. Cancer. 2009; 45:228–247. [PubMed: 19097774]

Online References

50. Pina C, Pignoni F. Tubby-RFP balancers for developmental analysis: FM7c 2xTb-RFP, CyO 2xTb-RFP, and TM3 2xTb-RFP. Genesis. 2012; 50:119–123. [PubMed: 21913310]

51. Moore M, et al. Phase I study to determine the safety and pharmacokinetics of the novel Raf kinase and VEGFR inhibitor BAY 43-9006, administered for 28 days on/7 days off in patients with advanced, refractory solid tumors. Ann. Oncol. 2005; 16:1688–1694. [PubMed: 16006586]

52. Kurzrock R, et al. Activity of XL184 (Cabozantinib), an oral tyrosine kinase inhibitor, in patients with medullary thyroid cancer. J. Clin. Oncol. 2011; 29:2660–2666. [PubMed: 21606412]

53. Clark JW, Eder JP, Ryan D, Lathia C, Lenz H-J. Safety and pharmacokinetics of the dual action Raf kinase and vascular endothelial growth factor receptor inhibitor, BAY 43-9006, in patients with advanced, refractory solid tumors. Clin. Cancer Res. 2005; 11:5472–5480. [PubMed: 16061863]

54. Sali A, Blundell TL. Comparative protein modelling by satisfaction of spatial restraints. J. Mol. Biol. 1993; 234:779–815. [PubMed: 8254673]

55. Durrant JD, Votapka L, Sørensen J, Amaro RE. POVME 2.0: An Enhanced Tool for Determining Pocket Shape and Volume Characteristics. J. Chem. Theory Comput. 2014; 10:5047–5056. [PubMed: 25400521]

56. McGann M. FRED pose prediction and virtual screening accuracy. J. Chem. Inf. Model. 2011; 51:578–596. [PubMed: 21323318]

57. Harder E, et al. OPLS3: A Force Field Providing Broad Coverage of Drug-like Small Molecules and Proteins. J. Chem. Theory Comput. 2016; 12:281–296. [PubMed: 26584231]

58. Li L, Li C, Zhang Z, Alexov E. On the Dielectric ‘Constant’ of Proteins: Smooth Dielectric Function for Macromolecular Modeling and Its Implementation in DelPhi. J. Chem. Theory Comput. 2013; 9:2126–2136. [PubMed: 23585741]

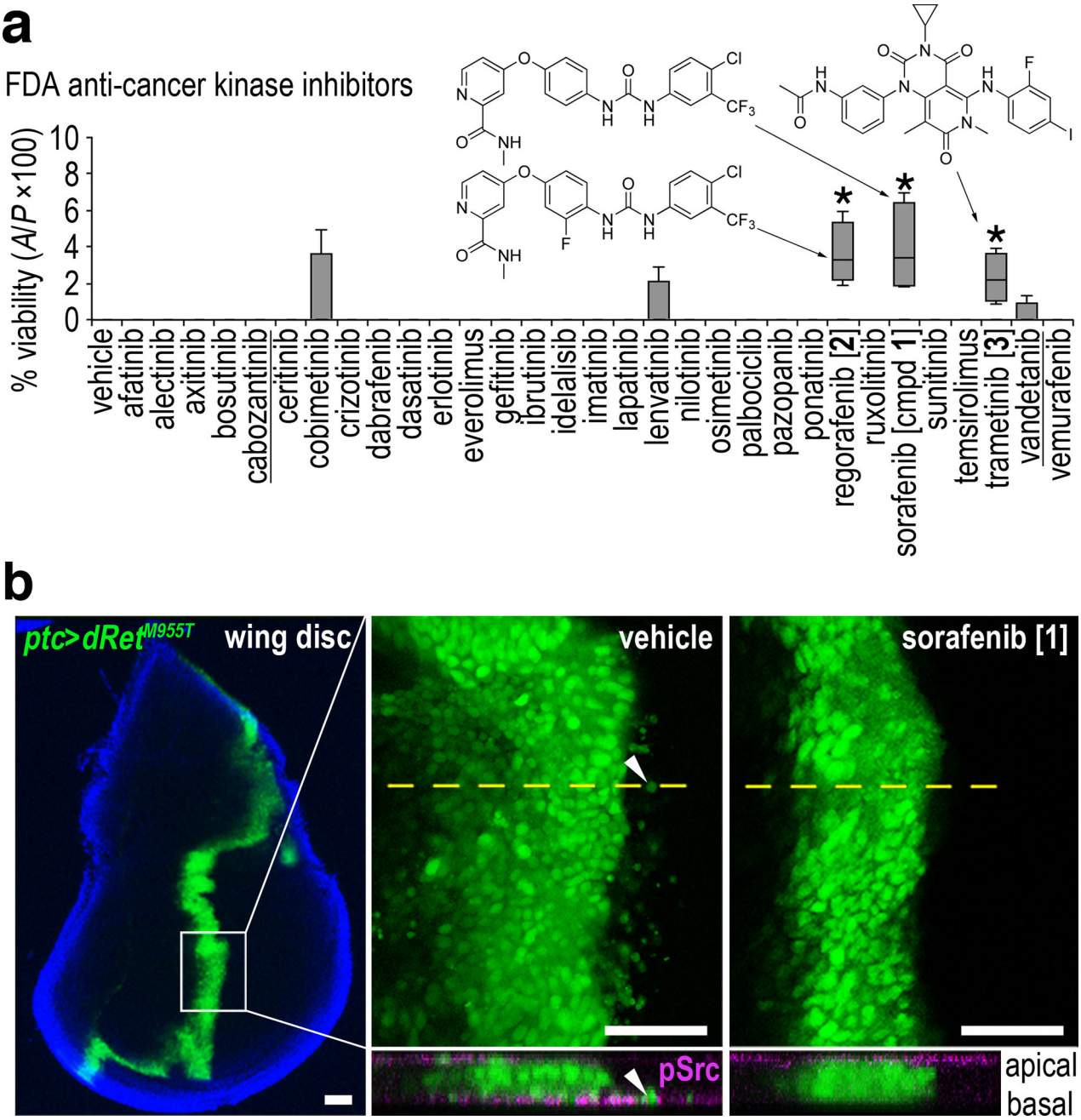

Fig. 1. Identifying sorafenib in drug screening using a *Drosophila* cancer model

a, Testing FDA-approved anti-cancer kinase inhibitors in *ptc>dRet*^{M955T} flies. Box-and-whisker plot shows minimum, 25th percentile, median, 75th percentile and maximum values. Two approved drugs for MTC are underlined. The best hit, sorafenib [**1**], promoted only ~5% rescue. Structures of top hits are shown. Asterisks, $p < 0.05$ in Student's *t*-test reflects comparison with DMSO vehicle control in quadruplicate.

b, *In vivo* cell migration assay. Left panel, a developing wing disc harboring GFP-labeled, *dRet*^{M955T}-expressing transformed cells. Blue, DAPI staining outlines the wing disc margin. Middle top and right top, magnified basal images for vehicle and **1** (400 μM) treatments,

respectively. Arrowhead, example of a migrating cell. Bottom, virtual z-series of confocal images derived from the plane indicated by dotted lines in top panels; tissues are stained for phospho(p)-Src (magenta). Arrowhead indicates a migrating transformed cell expressing pSrc basally. Scale bars, 50 μm.

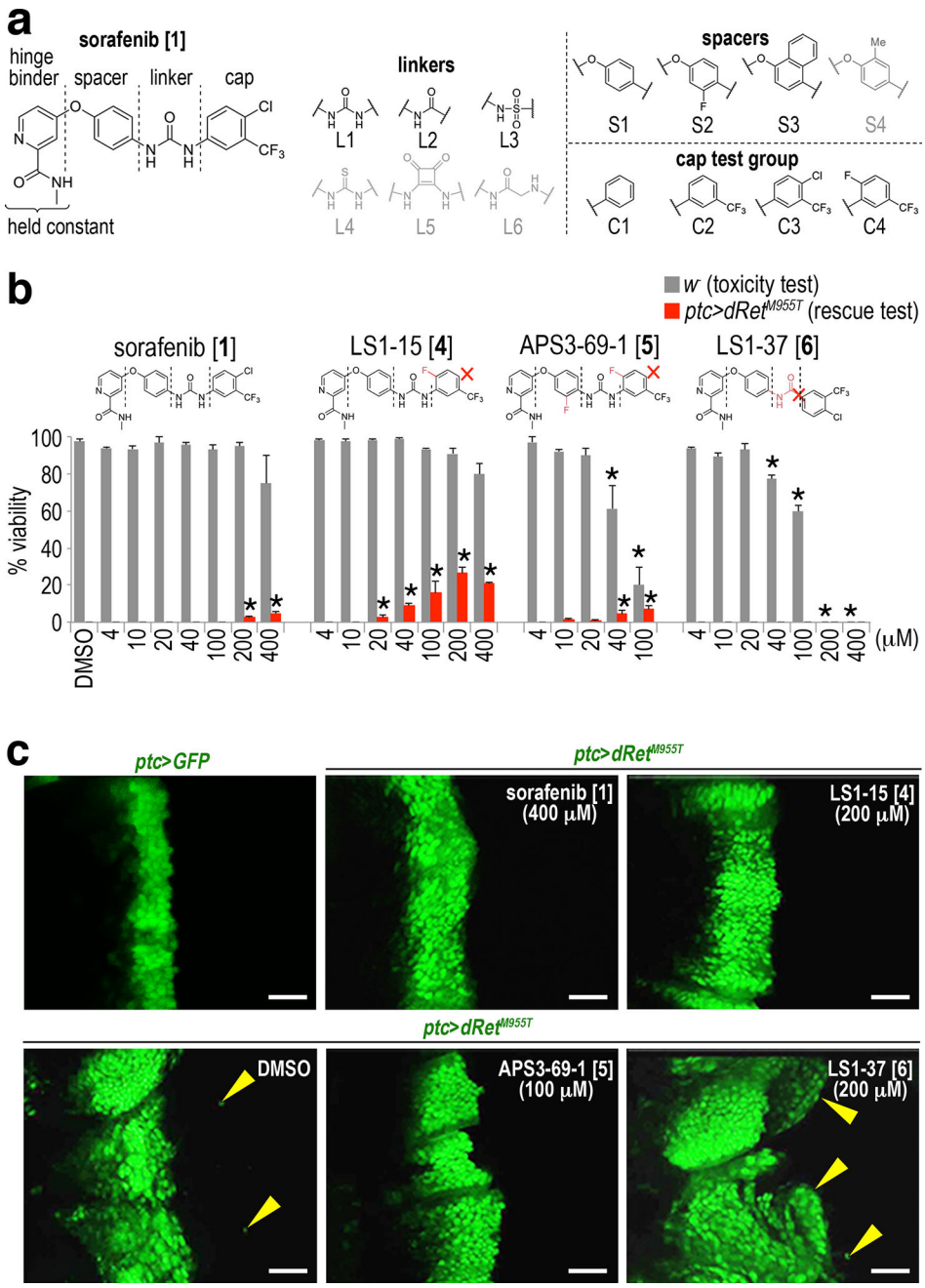

Fig. 2. Generation and efficacy of TCIs

a, The chemical structure of **1** and a conceptual fragmentation into four simple building blocks amenable to a modular synthetic strategy. The hinge binder was not altered in our studies. Gray structures: ineffective components as assessed in *ptc>dRet*^{M955T} animals.

b, Structure-activity relationships. Changes in TCIs with respect to **1** are highlighted in red, such as additional fluorines and an absent chlorine or –NH group. Distinct effects on whole body toxicity in non-oncogenic w^{-} flies (gray bars) and rescue of *ptc>dRet*^{M955T} flies (red bars) are highlighted below the chemical structures. Dosing 200–400 μM of **1** (93–186 μg/g

food) to flies is expected to give 1–2 μM of it in fly hemolymph. Error bars, standard errors in triplicate. Asterisks, $p < 0.05$ in Student's *t*-test as compared with no-drug control. **c,** Distinct effects of TCIs on cell migration. *ptc>GFP* is shown as control. Arrowheads, $dRet^{M955T}$-expressing, GFP-labeled transformed cells in wing discs migrating away from the *ptc* domain (apical views). Scale bars, 50 μm.

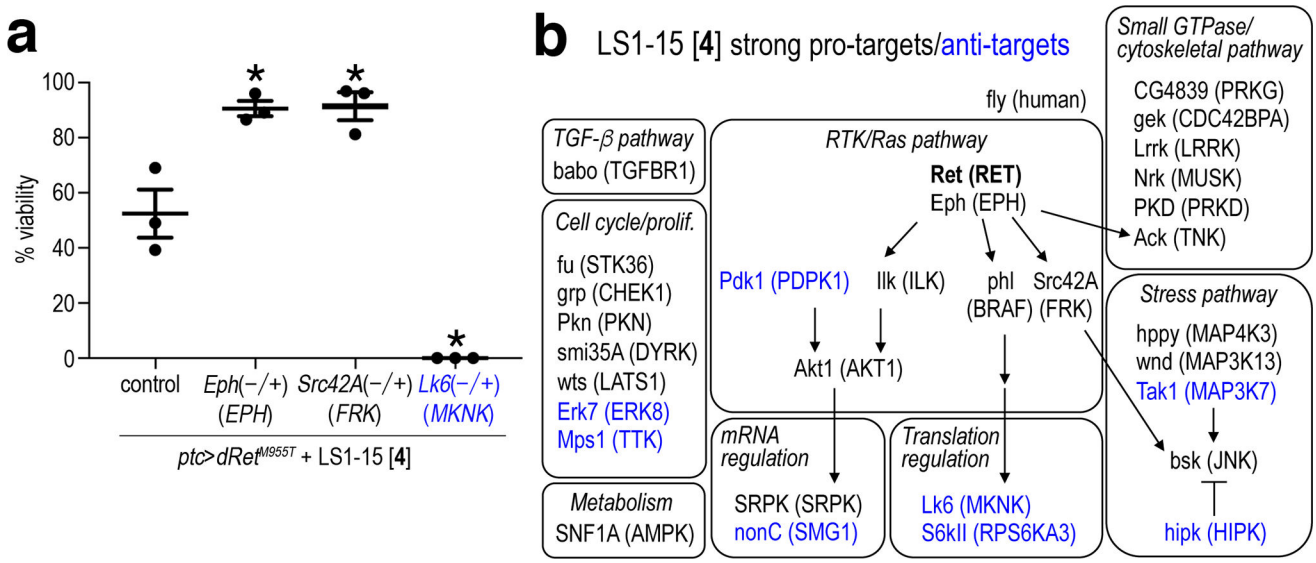

Fig. 3. Pro-targets and anti-targets for LS1-15 identified through genetic screening

a, Examples of pro-targets (Eph, Src42A) and an anti-target (Lk6) of LS1-15 [**4**]. Error bars, standard errors in triplicate. Asterisks, $p < 0.05$ in Student's *t*-test as compared with control. **b,** Representative signaling and cellular pathways defined by pro-targets and anti-targets of **4**. Shown are strong pro-targets and strong anti-targets giving > 91% and < 9% viability, respectively, as compared with ~50% viability of **4**-treated control flies at 23°C. Human orthologs are indicated (parentheses). Full data is presented in Supplementary Tables 2 and 3, and Supplementary Fig. 5. Blue, anti-targets.

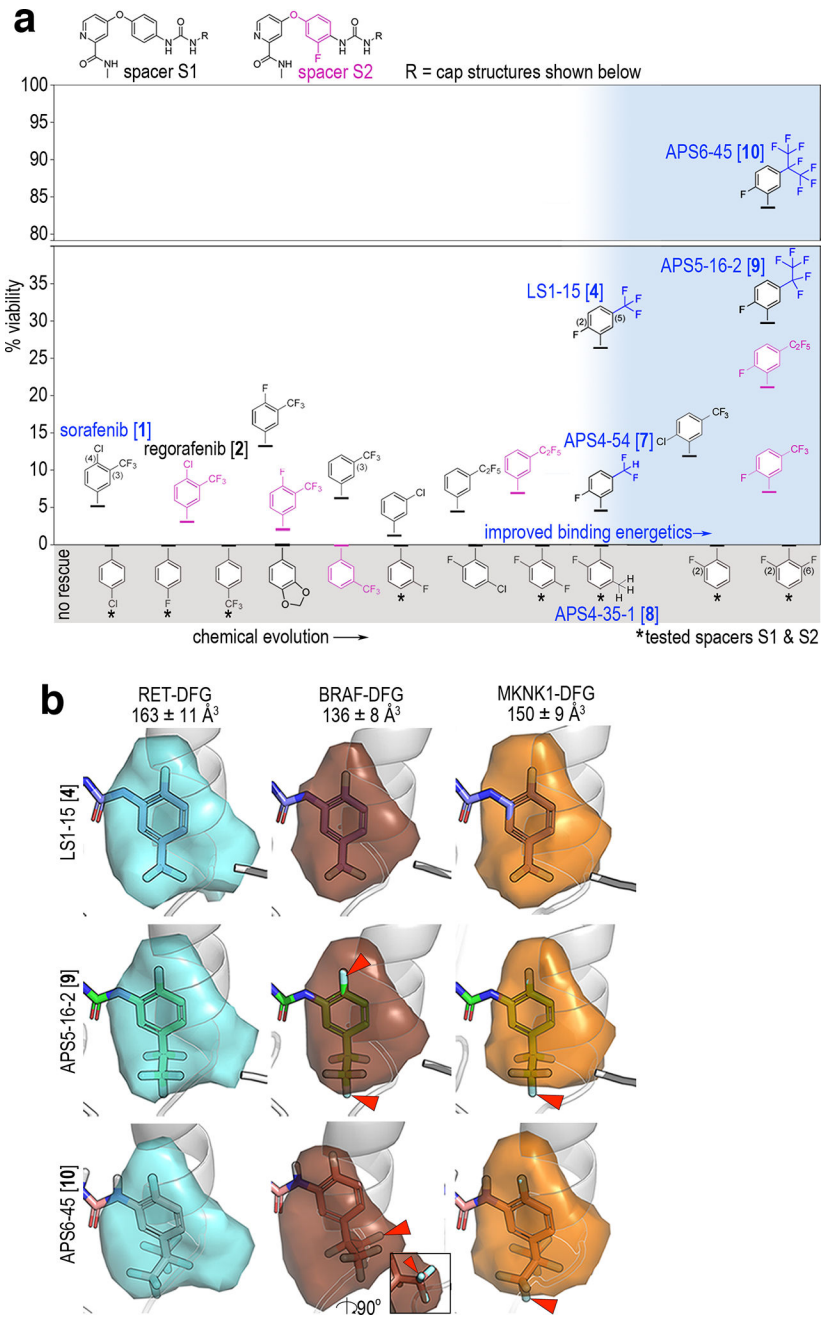

Fig. 4. Developing novel TCIs APS5-16-2 and APS6-45 by reducing activity towards BRAF and Lk6/MKNK

a, Chemical evolution of **1**. Alternate spacers S1 (black) and S2 (magenta) are shown at the top. X-axis indicates progressive modification of the cap (-R). Y-axis indicates percent rescue of *ptc>dRet*^{M955T} viability for each compound. White area: caps are evolved towards improved binding energetics (see Supplementary Fig. 11). Blue shaded area: related compounds showing specific SAR across perfluoroalkyl-substituted cap subgroups (blue). Gray shaded area: compounds that failed to rescue or were lethal; asterisks indicate no rescue for both S1 and S2 spacers. Optimal viability data as measured in Supplementary Fig. 2b are shown.

b, DFG-out subpockets of human RET, BRAF, and MKNK1 as determined by DFGmodel[31]. The DFG-pocket is contoured by a colored surface, and is superimposed with the cap of **4**, **9**, or **10**. Arrowheads indicate representative steric clashes between the caps and the pockets; inset for BRAF-DFG shows a lateral view of **10** to visualize clash. Mean +/− standard errors of volume calculations from 10 computationally derived models per kinase.

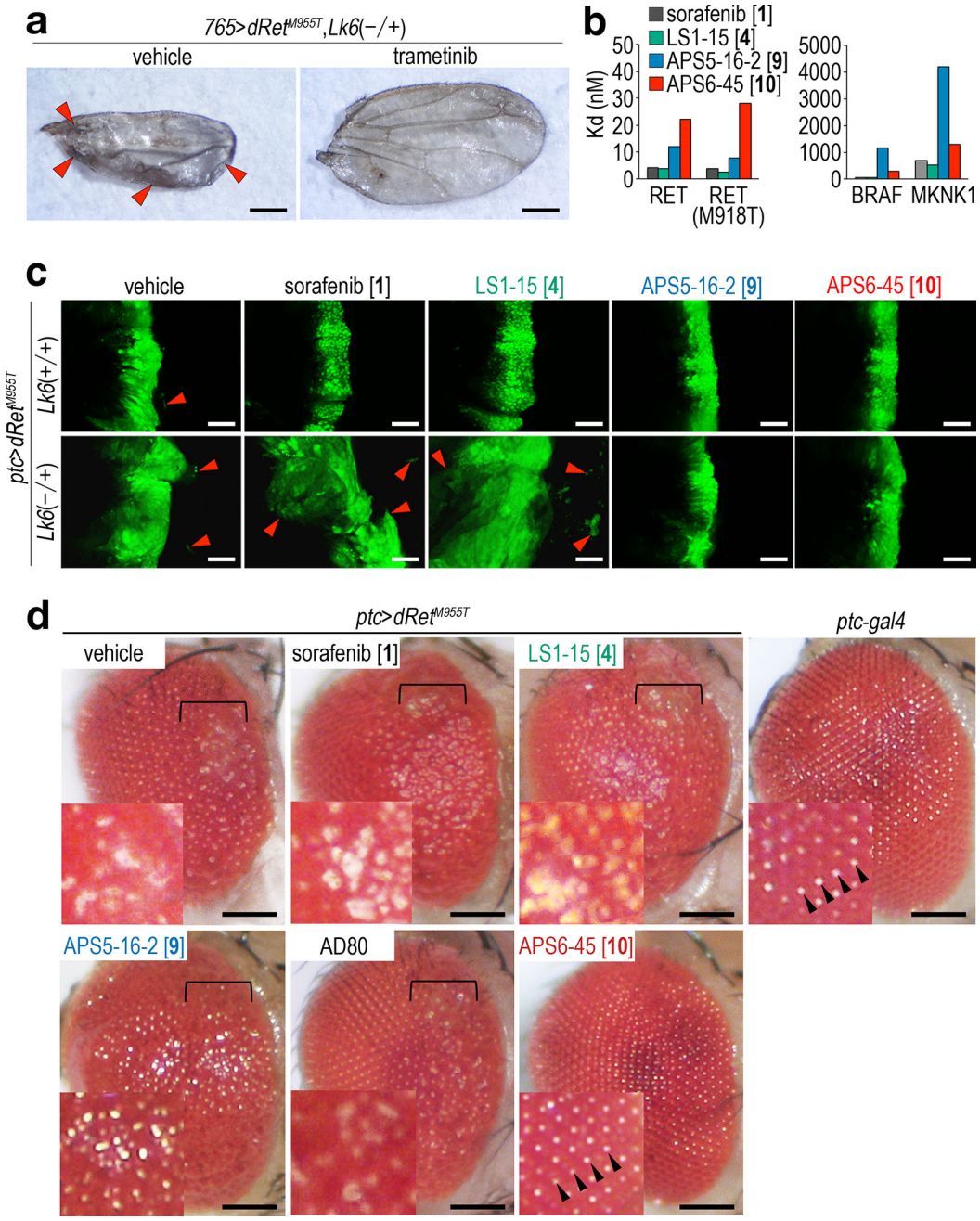

Fig. 5. Inhibition of RAS/MAPK signaling by APS6-45

a, *Lk6* mutation enhanced abnormal wing venation and affected overall wing structure. Arrowheads highlight excess wing vein materials. See Fig. 6a for controls. Scale bars, 500 μm.

b, Kd values for TCIs against human RET, its active mutant RET(M918T), and anti-targets BRAF and MKNK1. Note that Y-axis scales are 100-fold different between left and right panels. Averages in two independent assays are shown.

c, Effects on cell migration of reducing Lk6 in the presence of TCIs. Wing discs heterozygous for *Lk6* displayed enhanced *dRet*^{M955T}-induced cell migration, which was

further enhanced by **1** and **4** but not by **9** or **10**. Arrowheads, migrating cells (apical views). Drug concentrations: **1** (400 μM), **4** (200 μM), **9** (100 μM), and **10** (100 μM). Scale bars, 50 μm.

d, Effects of compounds on a fly rough eye phenotype; anterior is to the right. *ptc>dRet*^{M955T} exhibited a transformation-like phenotype including disarray of the ommatidial field in the anterior of the adult eye (brackets). **10** strongly rescued the rough eye phenotype, leading to smoothly arrayed ommatidia similar to *ptc-gal4* controls (arrowheads). Vehicle-treated control flies were dissected from pupal cases as they did not survive until adulthood. Insets, magnified views. Drug concentrations: **1** (400 μM), **4** (200 μM), **9** (100 μM), **10** (100 μM), and AD80 (100 μM). Scale bars, 100 μm.

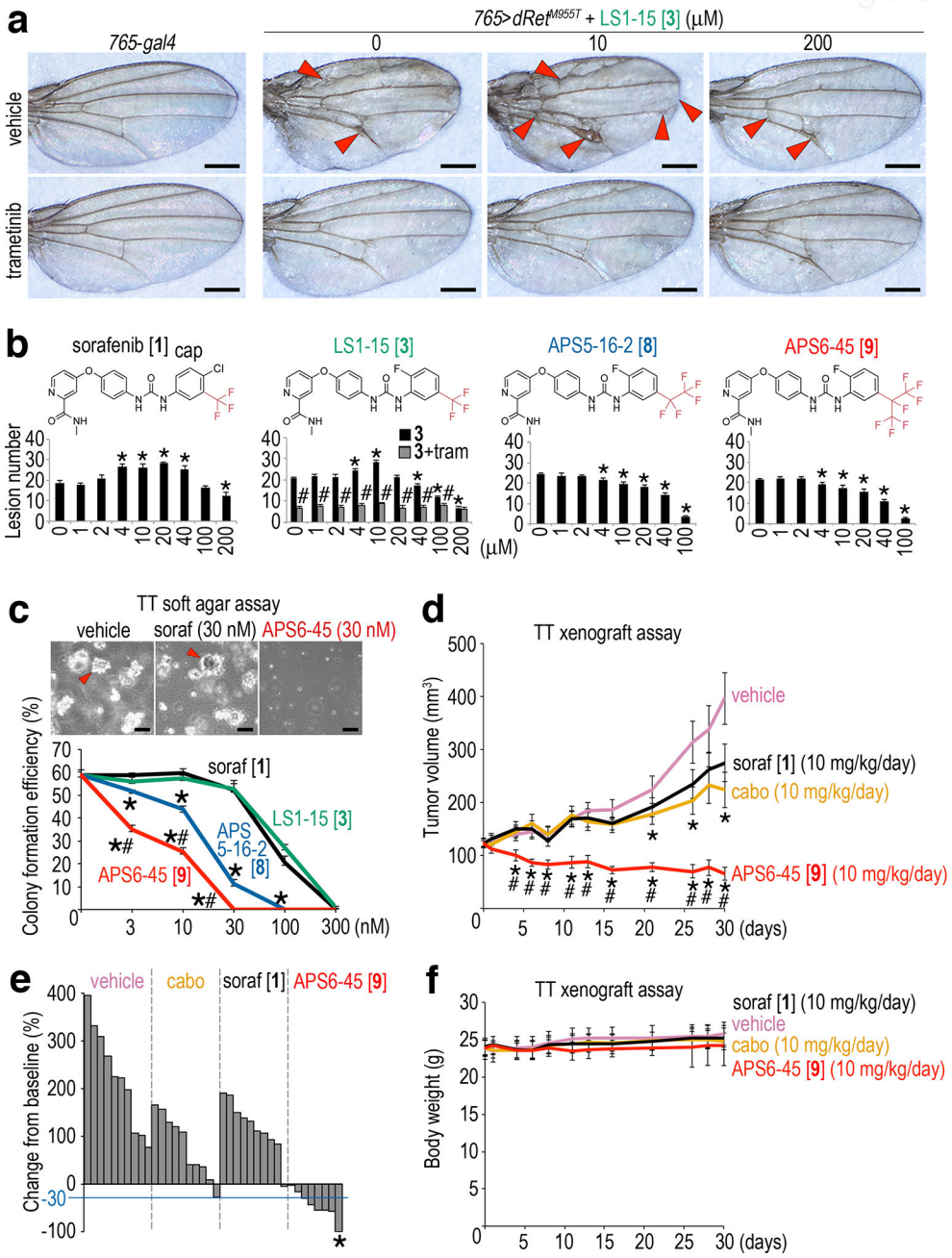

Fig. 6. The novel TCI APS6-45 displays exceptional *in vivo* efficacy

a, *765>dRet*^{M955T} adults exhibited ectopic vein material (arrowheads). Low-dose **4** enhanced ectopic venation and also notching of the wing margin (arrowheads); high dose suppressed both. **3** (1 μM) strongly suppressed ectopic venation. Scale bars, 500 μm.

b, Quantification of wing venation assays. **1** and **4** showed bipartite effects. tram, **3** (1 μM). Asterisks, $p < 0.05$ as compared with vehicle control. Pound signs, $p < 0.05$ as compared with **4** mono-treatment. Error bars, standard errors in triplicate.

c, TT cell colony formation in a soft agar assay was suppressed by **9** and **10**. Arrowheads, growing colonies. Scale bars, 100 μm. Error bars, standard errors in triplicate. Asterisks, $p <$

0.05 in Student's *t*-test as compared with **1**. Pound signs, $p < 0.05$ in Student's *t*-test as compared with **9**.

d–f, Oral administration of **10**, mouse TT cell xenografts.

d, In mouse xenografts, *in vivo* TT growth was more strongly suppressed by **10** than **1** (parent compound) or cabozantinib (MTC standard of care). Error bars, standard errors in 10 mice. Asterisks indicate $p < 0.05$ in Student's *t*-test as compared with vehicle control; pound signs indicate $p < 0.05$ in Student's *t*-test as compared with sorafenib and cabozantinib (cabo). Data from single experiment. **e,** Waterfall plot showing percent changes in tumor volume on day 30 relative to pretreatment baselines; each bar represents a single animal. The blue line indicates 30% tumor size reduction from baseline, a RECIST criteria[49]. Asterisk, complete response. Two mice were lost during the course of the experiment due to unknown causes.

f, Administration of **10** had no effect on mouse body weight. Same legend as **d**.